

# MWCNT-coated alumina micro-platelets for nacre-like biomimetic composites

Koen Evers<sup>a,\*</sup>, Harshit Porwal<sup>b</sup>, Richard I. Todd<sup>a</sup>, Nicole Grobert<sup>a,c,\*\*</sup>

<sup>a</sup> Department of Materials, University of Oxford, Parks Road, Oxford OX1 3PH, United Kingdom

<sup>b</sup> School of Engineering and Material Science, Queen Mary University of London, London, E1 4NS, United Kingdom

<sup>c</sup> Williams Advanced Engineering, Grove, Oxfordshire, OX12 0DQ, United Kingdom

## ARTICLE INFO

### Article history:

Received 11 October 2018

Received in revised form

9 January 2019

Accepted 17 January 2019

Available online 19 January 2019

## ABSTRACT

A novel building block material for the generation of non-brittle ceramic composites consisting of micron-sized alumina platelets homogeneously coated with multi-wall carbon nanotubes (MWCNTs) bound to their surface is described. The MWCNT phase is grown *in situ* from immobilised metal catalyst particles using chemical vapour deposition techniques. In-depth Raman and scanning electron microscope studies revealed that this approach solves the typical issue of MWCNT-agglomeration in ceramic matrices and paves the way to excellent control over MWCNT purity and concentration within the resulting composite material. Moreover, we show that the preparation of the catalyst is the most important factor for the generation of uniformly distributed MWCNTs of high-quality on these platelets. With these MWCNT-coated alumina building blocks, we have manufactured nacre-like biomimetic composites using spark plasma sintering. The resulting composites are electrically conductive and three-point bending tests show a transition from brittle/catastrophic failure to graceful failure, holding great promise towards multifunctional, tough and strong lightweight ceramic composite manufacturing.

© 2019 The Authors. Published by Elsevier Ltd. This is an open access article under the CC BY license (<http://creativecommons.org/licenses/by/4.0/>).

## 1. Introduction

Ceramics exhibit extraordinary material properties such as chemical inertness, high temperature resistance, hardness and strength. Despite these attractive properties, ceramics are of limited use for advanced engineering solutions [1], especially where major load-bearing is required. The reason for this lies in the low fracture toughness and hence extreme brittleness of ceramics. The biggest challenge in the development of ceramics with increased toughness [2] is that toughness increases often come at the expense of strength [3]. Nature has provided a solution to this challenge; several biomaterials have evolved to combine fracture toughness with strength. Nacre, for instance, has received much attention [4,5] as it combines both properties through its ‘brick-and-mortar’ microstructure [6]. Nacre possesses a hierarchical structure consisting of a hard phase of aligned  $\text{CaCO}_3$  platelets

approximately 0.3–0.5  $\mu\text{m}$  [7] thick and 5–10  $\mu\text{m}$  wide [3] combined with a soft biopolymer phase, allowing for several toughening effects to occur without compromising its strength [8–14]. Materials that mimic this microstructure of nacre have been developed aiming to increase the toughness of ceramics [15] and alumina ( $\text{Al}_2\text{O}_3$ ) platelets with the exact dimensions of platelets in nacre have been used to create a biomimetic nacre-like composite [16,17]. For example, Bouville et al. combined alumina platelets with a glassy ‘mortar’ phase to manufacture a strong and tough composite material [18]. Although exhibiting remarkable properties, these materials are far from optimal – it is likely that further improvements can be made by using nanomaterials that can introduce multifunctionality and further enhance mechanical properties. To improve upon this biomimetic design, multi-wall carbon nanotubes (MWCNTs) are suitable candidates to use as a functional reinforcement material in the ‘mortar’ phase. Due to the fibrous nature of MWCNTs they imitate the proteins found in nacre [19], and they have been shown to toughen ceramics significantly [20,21]. Moreover, MWCNTs can also be used to add functionality to a composite material. For example, they can increase the thermal [22,23] and electrical conductivity [24–26] of ceramic materials and can make them magnetic [27,28], yielding a multifunctional

\* Corresponding author.

\*\* Corresponding author. Department of Materials, University of Oxford, Parks Road, Oxford OX1 3PH, United Kingdom.

E-mail addresses: [koen.evers@materials.ox.ac.uk](mailto:koen.evers@materials.ox.ac.uk) (K. Evers), [nicole.grobert@materials.ox.ac.uk](mailto:nicole.grobert@materials.ox.ac.uk) (N. Grobert).

material. Whilst powder and colloidal processing methods have been the main strategies to incorporate MWCNTs in a ceramic matrix up to now [29], the dispersion of MWCNTs has proven difficult using these classical methods. Homogenous dispersions are attainable only at very low MWCNT concentrations (of at most a few wt%) whilst higher concentrations end up with severe agglomeration [26,30,31]. Agglomerated MWCNTs prevent densification and act as defects in the composite material [29]. Even if a reasonable dispersion is obtained, mechanical and chemical dispersion methods inherently rupture and introduce defects within the MWCNT structure resulting in a poor filler material. The growth of carbon nanotubes through a chemical vapour deposition (CVD) process can overcome the issue of an agglomerated and defective MWCNT-phase by growing the MWCNTs directly in or on ceramic scaffolds [32]. Here we show that by growing MWCNTs directly on alumina micro-platelets *in situ*, it is possible to create nacre-like building blocks that contain well-dispersed MWCNTs. This method yields a base material of alumina platelets that exhibit a homogeneous distribution of MWCNTs bound to the surface, paving the way to exploit the toughening mechanisms of both MWCNTs and platelets in ceramic composite materials. This scalable base material is suitable for application in well-established ceramic manufacturing processes such as gravitational sedimentation [33], direct pressing, freeze casting [34,35], and slipcasting [36] to create multifunctional and tough biomimetic MWCNT/ceramic composites. Alumina in conjunction with iron-based catalyst particles has been of particular interest as substrate material in the MWCNT field [37,38] as it offers increased MWCNT-growth rates compared to other substrates [39–42]. In this paper, the growth and distribution/dispersion of MWCNTs utilising iron-based catalysts on alumina platelets is optimised using acetylene-assisted CVD. Acetylene is a popular carbon precursor for MWCNT synthesis due to its low decomposition temperature (450 °C) [43,44]. Moreover, at higher temperatures, higher growth rates and MWCNTs exhibiting higher crystallinity are observed whereby 800 °C appears to be the optimum temperature [45–47]. We show that by controlling the catalyst annealing time, atmosphere and MWCNT growth synthesis parameters we can selectively grow well-dispersed, free-standing, high-quality MWCNTs (with an  $I_D/I_G$  ratio of  $0.54 \pm 0.04$ ) on  $Fe_2O_3$  nanoparticle infiltrated alumina platelets. Moreover, these MWCNTs are grown with a very low number of amorphous carbon by-products, as evidenced by absent 'D3' peaks in the Raman spectra [48]. The Raman spectra indicate superior quality over currently available commercial MWCNTs and most other CVD-grown MWCNTs. Aside from the low number of defects and high purity, the MWCNTs are shown to be non-agglomerated and well dispersed on the platelets. Having overcome the issue of MWCNT-agglomeration it is now viable to generate strong and tough ceramic composites that can fulfil the promise of the brick-and-mortar nacre-like microstructure. We show here that by using these MWCNT-coated alumina platelets, we are able to mimic the mechanical response of nacre and generate a non-brittle, tough and multifunctional ceramic composite.

## 2. Materials and methods

### 2.1. Alumina platelet/catalyst preparation for CVD synthesis of MWCNTs

Alumina platelets (Alusion™, Antaria Limited, Bentley, Australia, corundum, mean diameter 7.1  $\mu m$ ,  $D_{10}$  4.95  $\mu m$ ,  $D_{50}$  8.66  $\mu m$ ,  $D_{90}$  14.71  $\mu m$ , thickness 300–500 nm) were mixed with 2 wt% 20 nm flame spray pyrolysis-generated  $Fe_2O_3$  particles (Johnson Matthey Technology Centre, Reading, UK.) [49]. The catalyst particles were

either dry-mixed with the alumina platelets using a vortex mixer for 30 min [method A] or sonicated in a sonic bath (700 W) in ethanol for 30 min, after which the sample was dried in a vacuum oven overnight [method B].

### 2.2. CVD synthesis of MWCNTs on alumina platelets

A movable tube furnace was preheated to 800 °C. The furnace temperature was calibrated using a K-type thermocouple at the sample position to account for the difference between the furnace sensor and the temperature of the sample. Once the furnace reached the desired temperature, the furnace was shifted towards the sample located in a quartz tube (ID = 28 mm). With this approach, the alumina platelets infiltrated with catalyst particles reached 800 °C in 200 s in an exponential fashion rather than linearly, eliminating the long exposure of the catalyst particles during heat up of the furnace which is often seen in most other CVD MWCNT syntheses. Hence, using this method, the quality of the MWCNTs and MWCNT coverage can be directly correlated to the catalyst annealing times and annealing atmosphere at 800 °C. Annealing was carried out in an inert atmosphere with (500 sccm argon) for 0, 10, and 60 min for all platelets infiltrated with catalyst particles using method A and for 0, 10, 20, 30, 60, and 100 min for all platelets infiltrated with catalyst particles using method B. After the annealing treatment, the carbon precursor gas mixture at a flow rate of 1000 sccm was switched on for 10 min (4% acetylene, 96% argon). When hydrogen was included the flowrate was also maintained at 1000 sccm for 10 min (4% acetylene, 30% hydrogen, 66% argon). Platelets infiltrated with catalyst using method B, yielded the highest quality MWCNTs (determined by the  $I_D/I_G$  peak ratio in their Raman spectra) so for these platelets the annealing atmosphere was varied to explore its effect on the formation of MWCNTs. Annealing was done for 60 min under the following conditions: Inert (200 and 500 sccm argon), semi-inert (50 sccm argon), oxidising (0 sccm argon under airflow of 1620 sccm) and reducing (100 sccm argon/100 sccm hydrogen). After this annealing step, the precursor (4% acetylene, 30% hydrogen, 66% argon, total flow rate 1000 sccm) was switched on for 10 min.

### 2.3. Characterisation of nanomaterials

Raman spectra were obtained using a 25 mW,  $\lambda = 532$  nm laser (labRAM ARAMIS, Horiba instruments). The  $I_D/I_G$  peak intensity ratio was used to reveal the defectiveness of the as grown MWCNTs [48,50]. Each Raman spectrum is an accumulation of five spectra taken at one position. When reporting averaged Raman spectra, Raman spectra were collected at 5 different regions on the sample and averaged, with averaged  $I_D/I_G$  values reported  $\pm$  the standard deviation. Scanning electron microscopy (SEM) images were taken using 5 kV acceleration voltage on a JSM-840F (JEOL instruments). X-ray diffractometry (XRD) using a copper source was used to identify the structure of the catalyst particles before and after annealing treatment. TGA data were taken on a Netzsch STA 449 F3 Jupiter at 10 K/min in dry pure synthetic air, on MWCNTs grown on the platelets infiltrated using Method B, after a 60 min annealing step and 10 min precursor gas flow with 30% hydrogen. Resistivity measurements were conducted on a Jandel Four-point probe system with a probe spacing of 0.1 cm and currents of  $0.1 \times 10^{-3}$  and  $0.001 \times 10^{-3}$  A.

### 2.4. Ceramic composite manufacturing

After characterising the MWCNTs grown on the alumina platelets, the powder was loaded in a graphite die measuring 30 mm in diameter, and densified using spark plasma sintering

(FCT, HPD25/1, Germany) at 1600 °C for a dwell time of 5 min (heating rate 100 °C/min). The pressure was increased linearly to 42 MPa during heating and maintained at 42 MPa during the dwell time. After the sintering process, the sample was cooled at a rate of 100 °C/min and the pressure was reduced linearly. The disk was then polished and cut into 2 × 1.5 mm rectangular beams using a diamond saw following the 'Standard Test Method for Flexural Strength of Advanced Ceramics at Ambient Temperature' (ASTM C1161). Density measurements were done using Archimedes' principle. A Shimadzu loading frame with a 5 kN load cell was set-up with a three-point bend jig with a 20 mm span between bottom rollers, and the beams were loaded with a stroke speed of 0.5 mm/min. The exact same parameters were used to sinter and perform three-point bend tests on a control sample consisting of only pure alumina platelets. After failure, the tested beams were coated with 15 nm platinum and carefully transferred to a Zeiss Merlin high-resolution SEM to image the fractured region.

### 3. Results and discussion

#### 3.1. Effect of annealing and hydrogen inclusion

SEM analysis revealed minimal MWCNT growth on platelets prepared using method A that did not undergo annealing prior to MWCNT synthesis, indicating poor catalyst performance. However, complete activation of all catalyst particles was achieved by annealing in an inert atmosphere at 800 °C for 60 min, with most catalyst particles growing separated clumps of MWCNTs on the surface (Fig. 1). It is well established that hydrogen can significantly increase MWCNT yield in CVD when included in the carbon precursor mixture [51,52]. There are multiple arguments for this observation; hydrogen may prevent MWCNT growth termination by reducing the carbon influx, *e.g.* if the carbon at the surface of the catalyst is not removed fast enough compared to the carbon influx,

the surface becomes blocked and MWCNT growth will stop abruptly [51,53,54]. Hydrogen can also interact with the carbon precursor, modifying the decomposition rate [48]. Hydrogen inclusion at different concentrations during CVD growth has also been shown to change the size, shape and phase of iron catalyst particles [55]. Finally, hydrogen may play a role as an oxygen scavenger, creating water vapour, which has been shown to significantly extend catalyst lifetime [56]. In our experiments, when hydrogen was used during the synthesis, complete coverage of the platelets was achieved (Fig. 1). SEM images show that including hydrogen during synthesis enhances MWCNT growth by growing longer MWCNTs: This means that the catalyst is kept active for a longer time through either one or a combination of the mechanisms mentioned above.

For these platelets prepared using method A, the presence of defects in the MWCNTs depended on both the annealing time of the catalyst and the addition of hydrogen during MWCNT synthesis as revealed by the Raman  $I_D/I_G$  ratios (Fig. 2). The  $I_D/I_G$  ratio decreased with increased annealing time (Fig. 2a). When the catalyst was annealed for 60 min and MWCNTs were grown without hydrogen inclusion, an  $I_D/I_G$  ratio of  $0.82 \pm 0.04$  was measured (Fig. 2b). The addition of 30% hydrogen during MWCNT synthesis improved the  $I_D/I_G$  ratio to  $0.69 \pm 0.04$ . In addition, the presence of hydrogen resulted in sharp peaks in the Raman spectra; no signal in between the D and the G peak at around  $1500\text{ cm}^{-1}$  ('D3') was found, in contrast to samples produced without hydrogen. The absence of this peak is common in samples that are free of amorphous carbon [48]. Annealing platelets prepared using method A for 60 min in argon atmosphere and growing the MWCNTs using acetylene/hydrogen atmosphere thus yielded a highly pure, well-dispersed MWCNT phase with a low concentration of defects.

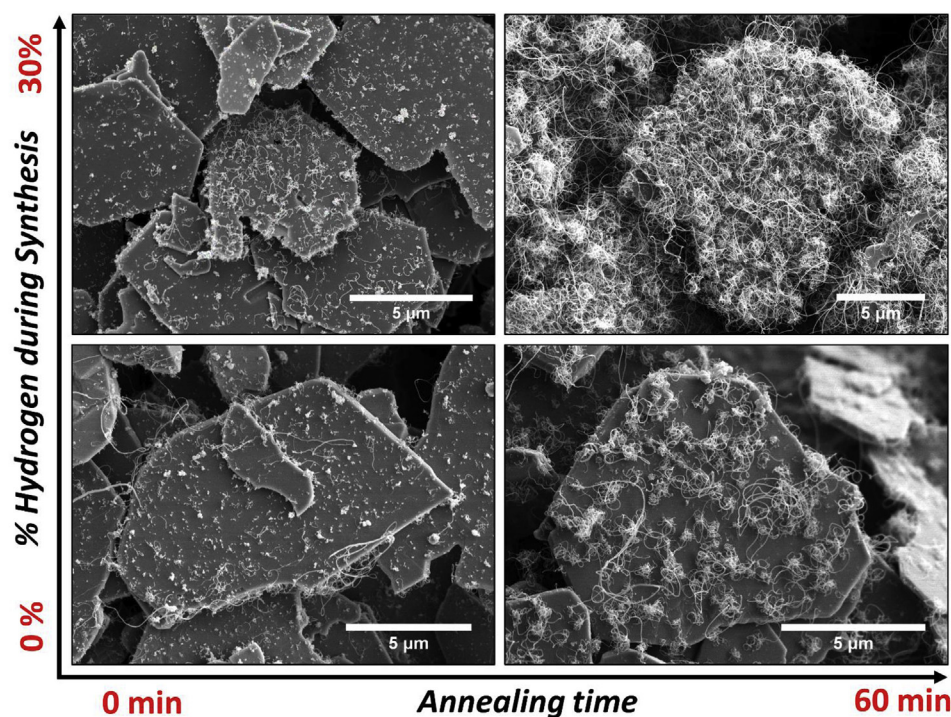
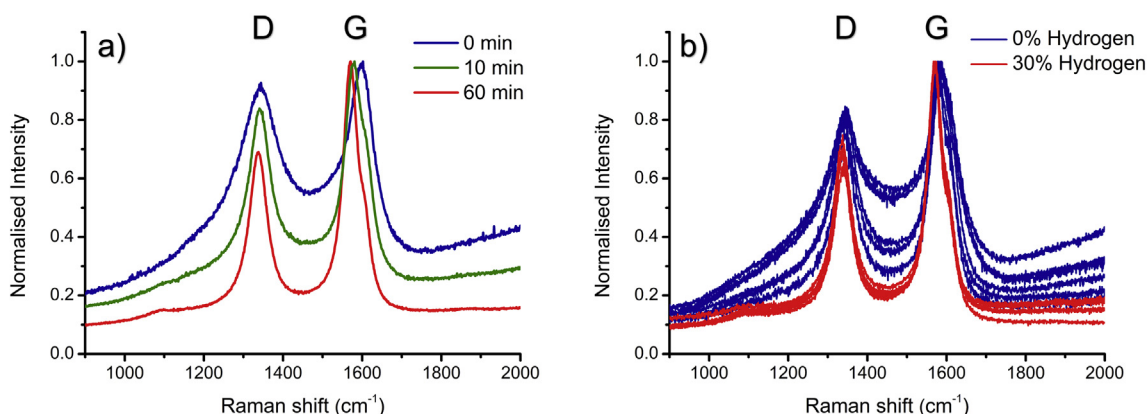


Fig. 1. SEM micrographs of MWCNT-coated alumina platelets, showing the effect of annealing before MWCNT synthesis, and the effect of including hydrogen during MWCNT synthesis. Platelets have been infiltrated with nanoparticles using catalyst infiltration method A.





**Fig. 2.** a) Averaged Raman spectra of MWCNTs grown with 30% hydrogen during synthesis, showing less defective MWCNTs after longer annealing times. b) Comparison of Raman spectra of MWCNTs grown after 60 min annealing, with and without hydrogen during synthesis. For both graphs the platelets are infiltrated with catalysts following method A.

### 3.2. Improvement using catalyst infiltration method B

Analogous to dry catalyst infiltration (method A), MWCNT growth on platelets with wet catalyst infiltration (method B) was inhibited without a catalyst annealing step, while complete surface coverage was obtained after sufficient annealing of the catalyst. From SEM images, we observe that increasing the catalyst annealing time increases the amount of MWCNTs grown (Fig. 3). After an annealing step of 20 min or more, the  $I_D/I_G$  peak ratio for MWCNTs grown on platelets prepared using method B was consistently  $0.54 \pm 0.04$  (Fig. 4a), a significant improvement in MWCNT-quality over those grown on platelets prepared using method A. Raw non-averaged Raman spectra of both catalyst infiltration methods are included here (Fig. 4b) to show that the  $I_D/I_G$  ratio improvement of platelets prepared using method B over platelets prepared using method A from  $0.69 \pm 0.04$  to  $0.54 \pm 0.04$  is consistent for each data point. This improvement in  $I_D/I_G$  ratio has

most likely to do with the removal of contamination in the powder during the sonication procedure in ethanol as the nanoparticle dispersion did not seem to be significantly improved with this step – some nanoparticle agglomerates could still be observed in the SEM.

### 3.3. Effect of annealing atmosphere on MWCNT crystallinity and growth

Having established that heat treatment/annealing has a significant effect on the catalyst particles and consequently the MWCNT-growth from these particles, we further investigated what effect this heat treatment has, e.g. what chemical state the catalyst particles are in when they grow MWCNTs. To answer this question, we forced the catalyst into either an oxidised or reduced state by manipulating the annealing atmosphere. While some sources report that oxidised iron species are favoured to catalyse MWCNT

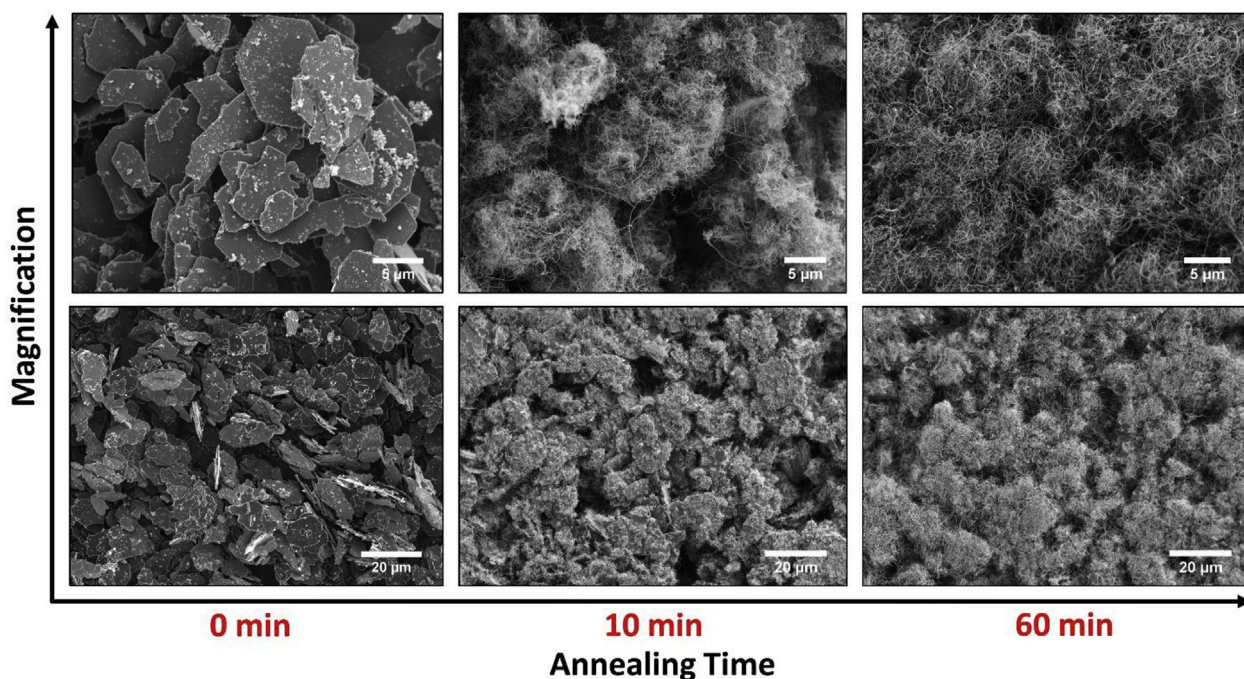


**Fig. 3.** SEM micrographs of MWCNT-coated alumina platelets, showing more MWCNT growth after longer annealing times. Platelets have been infiltrated with nanoparticles using catalyst infiltration method B.

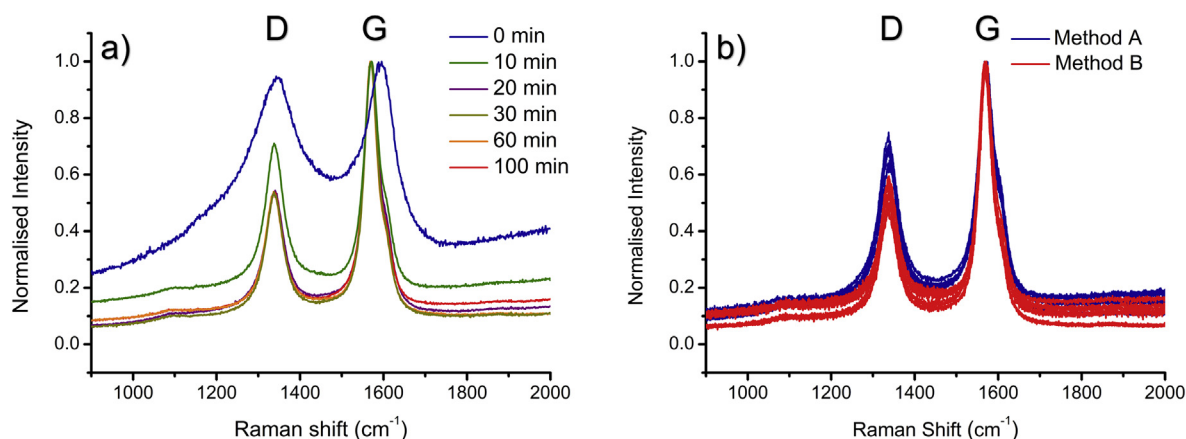


**Fig. 4.** a) Averaged Raman spectra of MWCNTs grown with 30% hydrogen during synthesis after different annealing times b) Comparison of Raman spectra of MWCNTs grown using catalyst infiltration method A and method B after 60 min annealing and hydrogen inclusion during synthesis.

growth [39,57], reducing iron oxide species during synthesis is most favourable according to more recent reports [58–61]. In the case of iron films, annealing and reducing results in both  $\gamma$ -Fe particles (FCC lattice, austenite) and  $\alpha$ -Fe particles (BCC lattice, ferrite), which are shown to have a different MWCNT growth mechanism [59] -  $\alpha$ -Fe grows MWCNTs through carbide formation while  $\gamma$ -Fe grows MWCNTs from the pure iron phase. For platelets prepared using method B, the effect of the annealing treatment on the catalyst particles in an oxidising, reducing and inert atmosphere is shown in Fig. 5. Annealing in a reducing atmosphere yielded inactive catalyst particles. While this seems to contradict the reports mentioned above, this can be explained by acknowledging the importance of the aluminium oxide support layer in MWCNT growth [62]; the reducing atmosphere may partially or completely reduce the alumina surface, effecting the interaction between the substrate and catalyst particle. The reduction of the alumina support layer is presumably much less of an issue in the case where deposited iron films cover the support layer. When we anneal in an oxidising atmosphere (such as in air or low argon flows), the resulting MWCNTs are low in quantity and less in quality

(Fig. 5). Optimal quality and quantity is observed with an argon flow of 200 sccm and greater. This most likely indicates that in our setup this is the minimum flow rate to ensure an inert atmosphere. The need for an inert atmosphere during annealing is shown by the combination of SEM and Raman data in Fig. 5, where it is seen that a non-uniform MWCNT-coverage and defective MWCNTs are obtained when a non-inert atmosphere is used during annealing. It is clear from these experiments that for high-quality MWCNT growth catalysed by  $\text{Fe}_2\text{O}_3$  nanoparticles on alumina, annealing in an inert atmosphere is a prerequisite. From our analysis however, we cannot make any conclusion on what oxidation state the catalyst particles are in when they grow MWCNTs. It is possible that the catalyst sites are in a reduced oxidation state due to the carbon precursor when MWCNT synthesis is commenced, as it has been shown previously that oxidised Fe can be reduced by acetylene exposure during CVD by hydrogen atoms liberated from hydrocarbon decomposition [53,63]. To better understand what happens to the catalyst particles during the annealing step in inert atmosphere, we have taken a closer look at their structure.

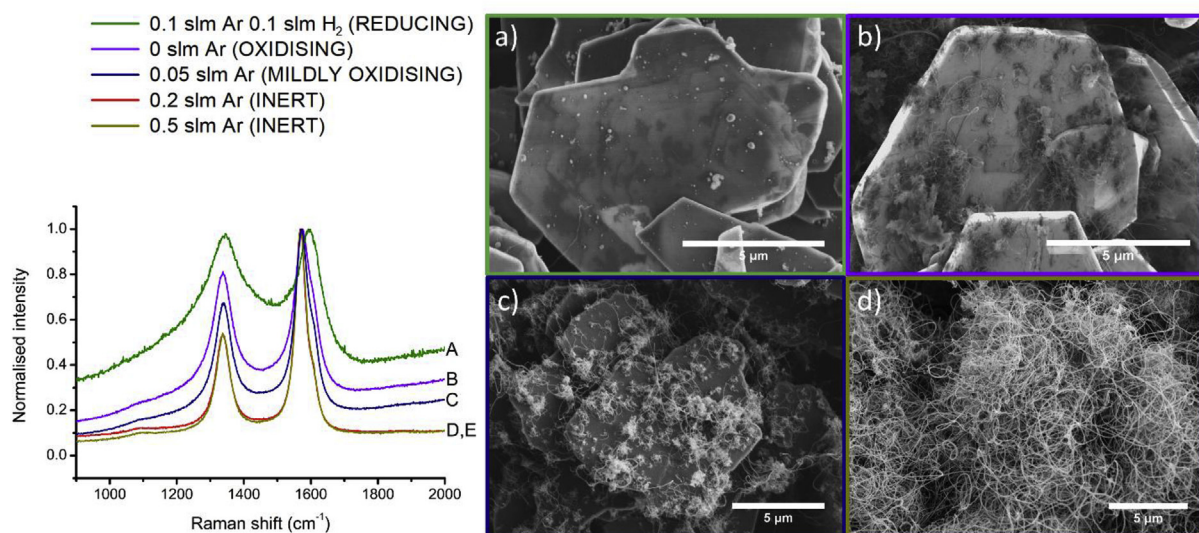


**Fig. 5.** Raman spectra showing the effect of the chemical atmosphere during annealing. SEM micrographs correspond to CNT growth under a) reducing, b) oxidising, c) mildly oxidising and d) inert atmosphere.



### 3.4. Spinel formation and catalyst immobilisation

Usually, tailoring the chemical state of individual nanoparticles through annealing is discouraged because of coalescence and Ostwald ripening, which has been stated to be one of the limiting factors in continued MWCNT-carpet growth [64,65]. In contrast, we observe that annealing the  $\text{Fe}_2\text{O}_3$  catalyst particles on the alumina platelet surfaces enhances MWCNT quality and yield, with no significant coalescence occurring and with the catalyst particles immobilised on the alumina surface (Fig. 6). The immobilisation of  $\text{Fe}_2\text{O}_3$  nanoparticles has been shown before by Homma et al. [66] on a  $\text{Si}(001)$  substrate, where pure iron nanoparticle catalysts were shown to agglomerate while  $\text{Fe}_2\text{O}_3$  nanoparticle particles did not, even at temperatures of  $950^\circ\text{C}$ .

The ability of  $\text{Fe}_2\text{O}_3$  nanoparticles to facilitate MWCNT growth without coalescing is reproduced here on an alumina surface. Kaneko et al. [67] reported impaired diffusivity of iron on alumina substrates where iron-based catalyst particles are seen to dissolve in the alumina substrate during annealing. We believe that this insight is key to understand the immobilisation and catalytic activity of  $\text{Fe}_2\text{O}_3$  nanoparticles on alumina supports. While some researchers believe that chemical bonding between a metal catalyst and substrate would prevent the catalytic behaviour of the metal [68], we propose that the iron oxide phase plays a strong role in the formation of an immobilising chemical bond with the alumina surface as indicated by the observed lack of coalescence of nanoparticles on alumina platelets. XRD spectra in Fig. 7 show that the haematite ( $\text{Fe}_2\text{O}_3$ ) nanoparticles were converted to hercynite ( $\text{FeAl}_2\text{O}_4$  spinel) in an inert atmosphere. At the same time the XRD spectrum shows that the original nanoparticle phase, haematite, disappears in the annealed sample, indicating a full conversion. In a similar way  $\text{Co-Al}_2\text{O}_3$  spinel structures have been found before on  $\gamma$ -alumina substrates after annealing [69] which have been suggested to stop catalytic activity [70].

In our case, we conclude that the opposite is the case and that the formation of the spinel structure is vital to prevent Ostwald ripening and grow a high quality, well dispersed MWCNT phase. SEM images of annealed catalysts before and after TGA clearly show that the catalyst particles have diffused into and/or reacted with the substrate (Fig. 6). After burning off the MWCNTs, the catalyst sites show holes in the structure which resemble the diameter of the grown MWCNTs and are presumably sites where the MWCNT was attached. From the TGA curve we determine that the amount of MWCNTs grown on platelets prepared using method B was 21 wt%. The decomposition temperature of the as-grown MWCNTs was  $666^\circ\text{C}$ .

### 3.5. Biomimetic fracture toughening mechanisms in alumina platelet brick-and-mortar structures

When pure alumina platelets without the MWCNT-coating were sintered and tested in 3 pt bend, the load-displacement curve (Fig. 8) shows that after an initial brittle zone, further crack growth is resisted – presumably due to interlocking of platelets. SEM revealed thickened platelet-like structures with a thickness around 5–10 times that of the platelets pre-sintering (Fig. 9b). The thickened platelets were aligned in a nacre-like brick-and-mortar structure. These structures dissipate fracture energy through a very tortuous crack path (Fig. 10a) and show crack branching and crack deflection (Fig. 10a and b), platelet-interlocking (Fig. 10c), as well as crack deflection around platelets and crack bridging (Fig. 10d). In contrast with non-biomimetic/conventional alumina which breaks violently in a brittle fashion and shows a straight crack with both pieces being catapulted from the bending rig, both the pure alumina platelet and MWCNT-coated platelet composites have wavy fracture surfaces (Fig. 9a and c), show tortuous crack paths and hold together on the bending rig after failure, accentuating their non-brittle nature.

### 3.6. Densification of MWCNT-coated alumina platelet composites

For fair comparison, the same sintering conditions were used for all samples. However, sintering conditions used for pure alumina platelets did not provide a fully densified composite when sintering the MWCNT-coated platelets. While platelet-only structures were 95–98% dense, those with MWCNTs were 80–95% dense and show voids in the structure (Fig. 9d), which may act as fracture-initiating defects. As a result, lower strengths were obtained (Fig. 8). The strength values were further depressed by the difficulties in polishing such relatively porous structures – a perfectly polished surface was not obtained and thus imperfections at the surface may also lead to crack initiation below the ideal strength of the composite. Lastly, we note the relatively large volume fraction of CNTs in these composites of 21 wt% (Fig. 6) compared to nacre which has an organic phase content of 5 wt% [4,71]. It is very likely that the strength of these composites can be improved by tailoring the MWCNT length and coverage in CVD; the CNT-phase can be modified by reducing the length of CNTs through reducing the carbon precursor exposure in CVD or reducing the amount of grown CNTs by infiltrating the platelets with a smaller amount of catalyst particles. This will not only improve the density of the final composite but will yield a microstructure that more closely resembles nacre. We note that the produced MWCNT-coated alumina platelet composites in this work show the feasibility and

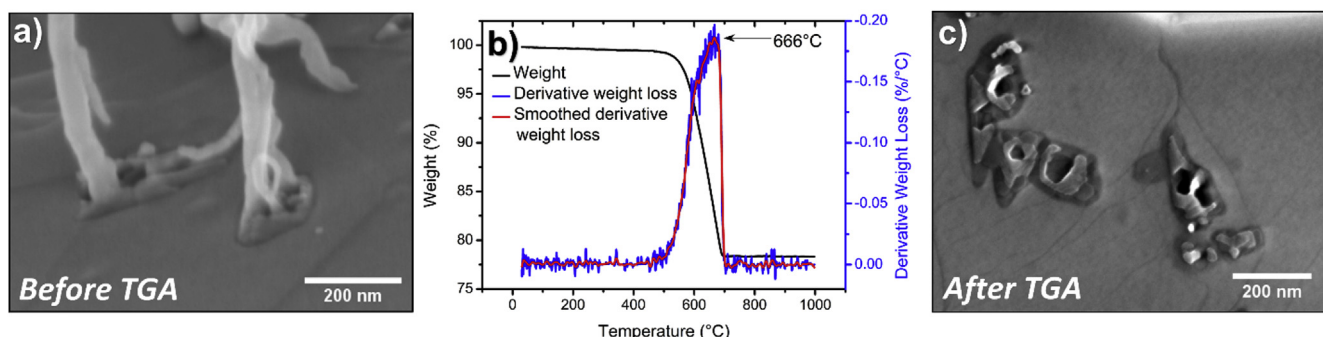
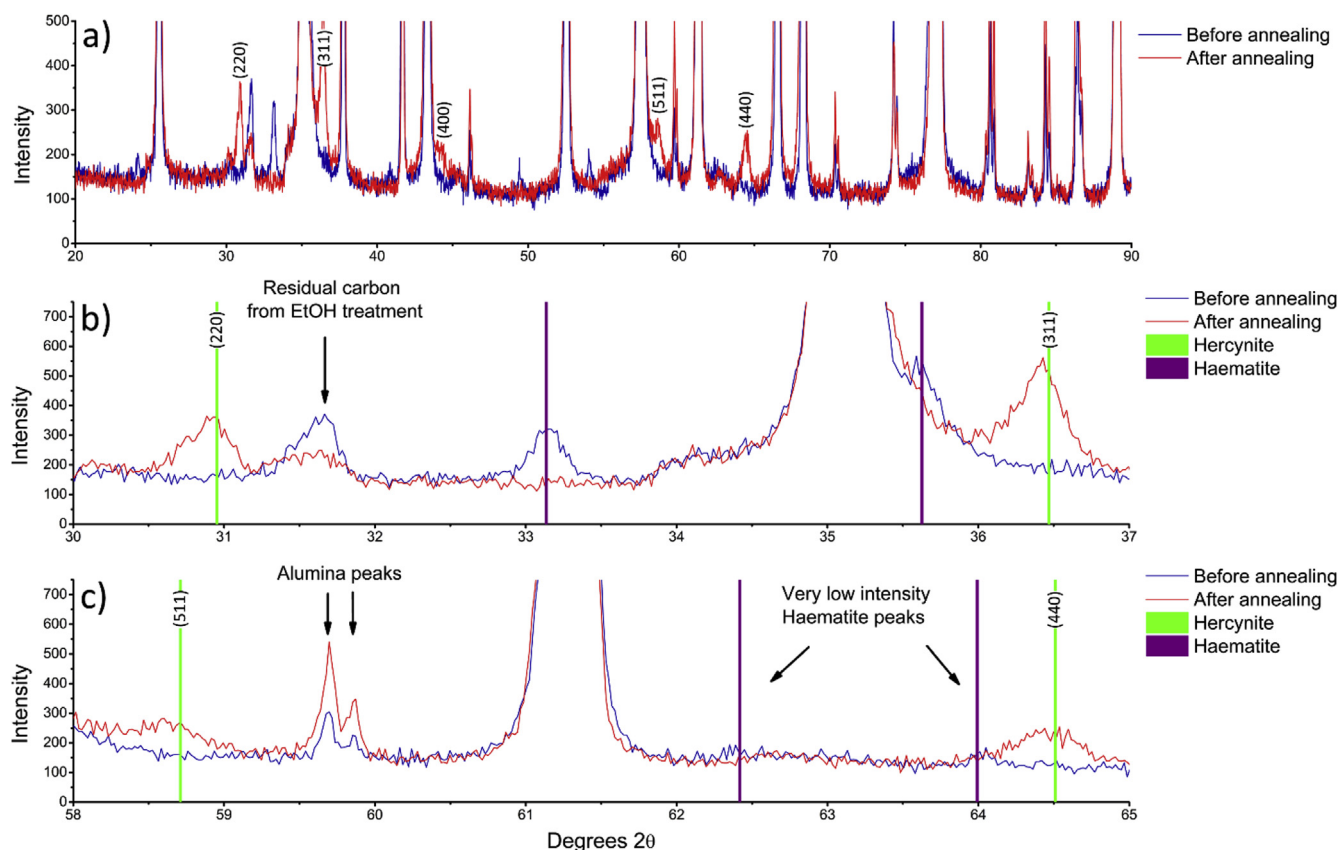
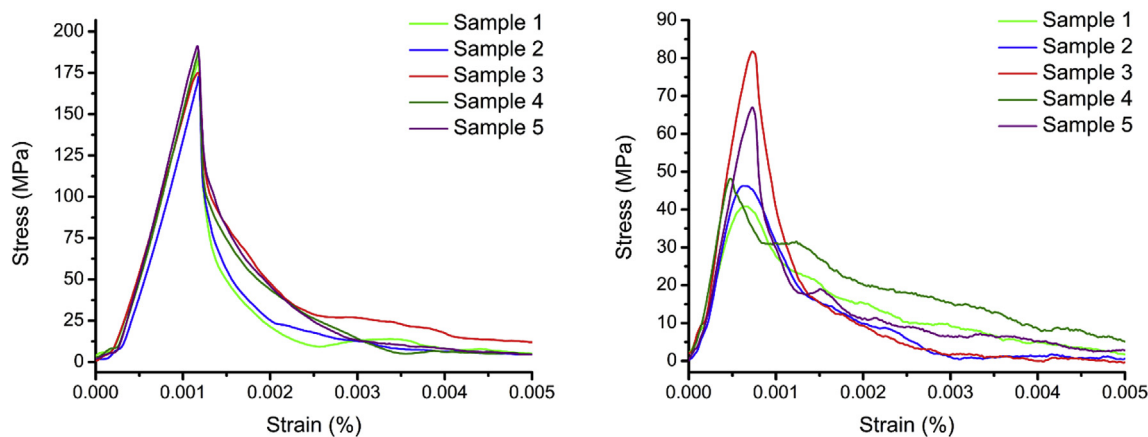


Fig. 6. a) SEM micrograph of a catalyst site before TGA b) TGA curve showing weight loss between 500 and 700 °C and c) SEM micrograph of a catalyst site after TGA.



**Fig. 7.** a) XRD Spectra of alumina platelets infiltrated with catalysts following method B, before and after annealing for 60 min in inert atmosphere, showing hercynite peaks appearing after annealing (labelled) b-c) A zoom-in of the XRD spectra showing that hercynite peaks show exclusively in the annealed powder while haematite peaks show exclusively in the powder which did not undergo annealing, thus indicating a conversion from haematite to hercynite during the annealing procedure (the large peaks in between are from the large alumina background and are cut off in the y-direction to better show the peaks originating from the 2 wt% nanoparticle volume).



**Fig. 8.** Mechanical response in 3 pt bend testing of samples of a) Alumina in a brick-and-mortar structure of aligned platelets and b) MWCNT-coated alumina platelet composites.

advantages of combining alumina platelets with CNTs *in-situ* and are by no means a final and optimised product.

### 3.7. Properties of MWCNT-coated alumina platelet composites

There are several notable improvements that the MWCNT-coated alumina platelet composites have over the alumina platelet only ceramics. Most importantly, load-displacement data (Fig. 8) reveals that composites made with MWCNT-coated alumina

building blocks do not have an initial brittle zone but fail in a completely non-brittle fashion, showing a stable graceful failure from the onset of fracture which mimics the mechanical response of nacre in 3 pt bend completely. We observe that the CVD-grown MWCNTs act as a spacer and prevent the platelets from sintering into thicker platelet structures (Fig. 9b and d). From this observation we believe that the catalyst particles located at the origin of the MWCNTs play a minimal role in the mechanical response of the composite other than the attachment of the MWCNTs. A

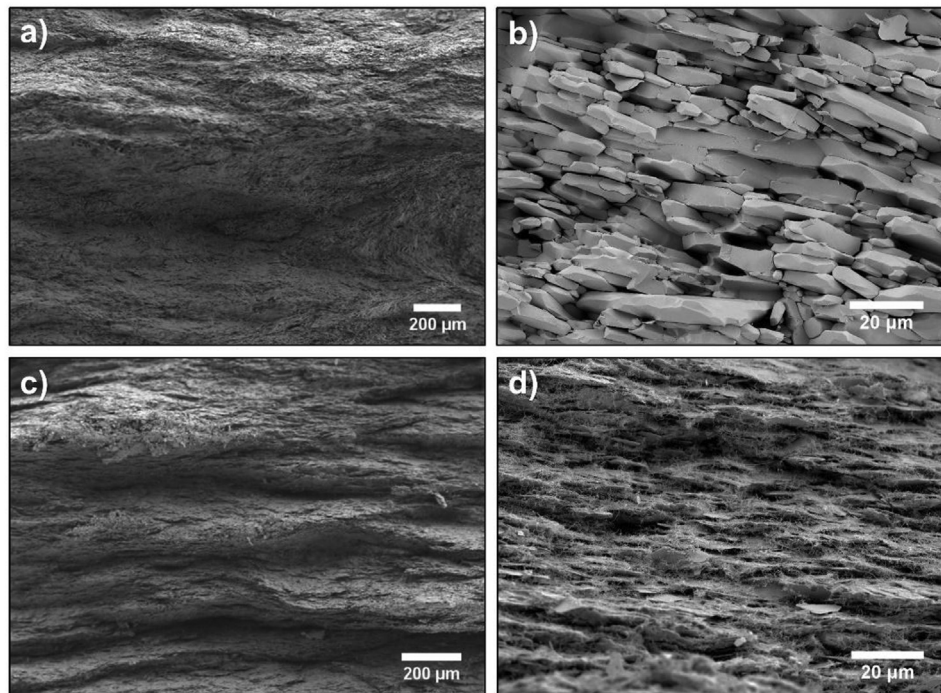


**Fig. 9.** SEM micrographs of a fracture surface of a broken beam of a-b) densified alumina platelets and c-d) densified MWCNT-coated alumina platelets.

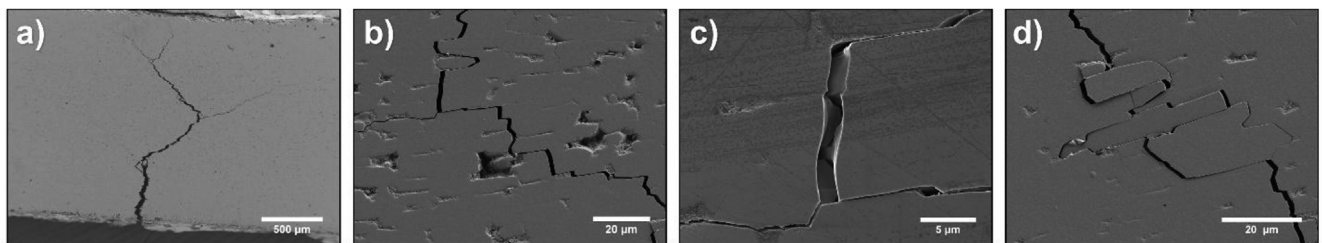


**Fig. 10.** SEM micrographs of a polished beam of sintered alumina platelets after 3 pt bend testing, taken from the side of the beam, showing a) macroscopic crack branching and deflection b) microscopic crack branching and deflection c) platelet-interlocking and d) crack bridging.

maintained small platelet-size allows for platelet-platelet interactions such as interlocking and sliding to occur on a 5–10 $\times$  smaller scale than when grain growth occurs. In addition, the MWCNTs grown from the catalyst particles are well attached to the platelets as evidenced by crack-bridging mechanisms where MWCNTs are stretched in between two crack surfaces (Fig. 11a). Evidence of this extrinsic toughening is seen up to large crack

surface separations of tens of microns where longer tubes are still bridging the crack (Fig. 11b). MWCNTs are seen to be embedded in the alumina surface (Fig. 11c) which can improve these toughening effects.

Since we observe stable fracture for the MWCNT-coated alumina platelet composites, we can obtain a quantitative measure of this toughening by determining the work of fracture  $\gamma_f$ . The work of

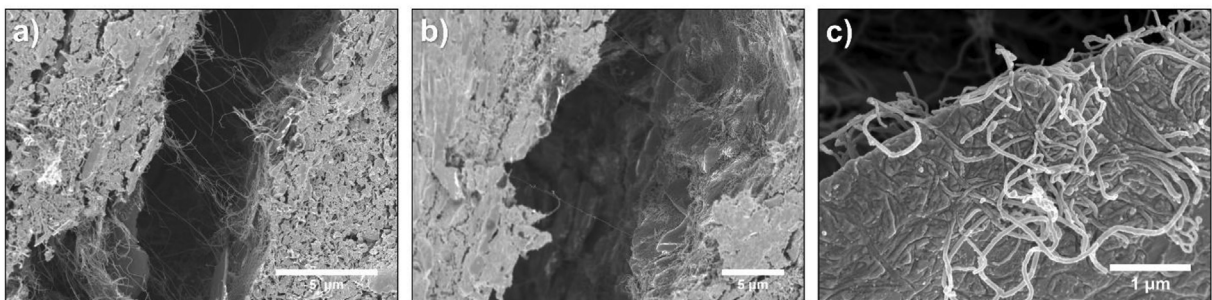


**Fig. 11.** SEM micrographs of a sintered and polished beam of MWCNT-coated platelets showing a) crack-bridging of stretched MWCNTs over distances of around a) 5  $\mu$ m and b) 20  $\mu$ m. c) SEM micrograph of a MWCNT-coated alumina platelet after sintering, showing a modified surface as a result from the SPS procedure.



fracture is defined as the area under the load-displacement curve of a specimen in stable fracture, divided by twice the cross-sectional area of that specimen and is between 67 and 106 J/m<sup>2</sup> (An average of 80 J/m<sup>2</sup> over 5 measurements) for the composites in Fig. 8b. Monolithic alumina has a fracture toughness  $K_{IC}$  between 3.0 and 6.0 MPa√m and a Young's modulus  $E$  between 410 and 380 GPa<sup>80</sup>. Using the Griffith energy criterion for crack growth, we note that the critical mechanical-energy release rate,  $G_c = 2\gamma_f = K_{IC}^2/E$ <sup>73</sup>. Monolithic alumina therefore has a work of fracture between 11 and 47 J/m<sup>2</sup>. The MWCNT-coated alumina platelet composites show a significantly higher work of fracture which is in agreement with the observed toughening mechanisms.

The MWCNT-coated platelets also have great potential as fillers in epoxy and polymer matrix composites<sup>37,76,77</sup>. In addition, these intercalated MWCNT networks can potentially be used to monitor the formation of defects and cracks, or as a Joule heater<sup>78</sup>. As MWCNTs have been shown to increase electrical conductivity in non-biomimetic composites before<sup>26–28,79</sup>, we have proceeded with resistivity measurements of the MWCNT-reinforced composites, which yielded values between 0.16 Ωcm (high current) and 1.03 Ωcm (low current). These values accentuate the potential for application in a multifunctional composite.

Optimising the sintering procedure, using shorter MWCNTs or introducing a third phase are all promising manufacturing routes toward a fully dense nacre-like MWCNT-reinforced ceramic that is toughened and non-brittle while maintaining a high strength.

#### 4. Conclusion

MWCNT growth on micron-sized alumina platelets has been investigated. For Fe<sub>2</sub>O<sub>3</sub> catalyst particles on the alumina platelet surface, long annealing times improved the yield and quality of the subsequently grown MWCNTs. We found that during annealing in argon atmosphere, the Fe<sub>2</sub>O<sub>3</sub> particles reacted with the alumina platelet surface to form hercynite. The lack of coalescence during these long annealing times indicates that the hercynite formation gives a degree of immobility to the catalyst sites, resulting in a well-dispersed and homogeneous MWCNT-coverage. The catalyst sites grow high quality and quantity MWCNTs when annealed in argon for more than 20 min at 800 °C, and by including hydrogen during synthesis we can consistently grow MWCNTs with a  $I_D/I_G$  ratio of  $0.54 \pm 0.04$ . Exposing the Fe<sub>2</sub>O<sub>3</sub> catalyst particles to high temperature in an oxidising or reducing environment yielded very poor MWCNT growth. Annealing in inert argon atmosphere for sufficient time (>20 min) before MWCNT synthesis is shown to be essential for the activation of these catalyst particles on alumina surfaces and key to growing a high coverage of well distributed MWCNTs on the platelets. We have shown that these MWCNT-coated platelets can be used as a building block for ceramic composites. Various toughening mechanisms are active due to the combination of platelets and MWCNTs. By addition of the MWCNTs we have shown a complete transition from brittle failure to graceful failure. Although the strength of the MWCNT/platelet composite is only about half of that of the platelet-only ceramic, they are much tougher and lighter, and their strength is already at a usable level. The non-catastrophic failure as well as the increased conductivity and reduced weight are advantageous properties. Furthermore, the demonstrated scalable approach to grow a homogeneous and pure MWCNT coating on alumina is an attractive alternative to other CNT reinforcing techniques whereby the MWCNTs are often damaged during the dispersion procedure. The shown infiltration method is applicable to create MWCNT/Alumina platelet building blocks with different aspect ratio's and different shapes to generate a range of tailored MWCNT-reinforced composite structures.

#### Acknowledgements

The authors are thankful to Dr. Phil Holdway for his help with taking the XRD spectra. We are also grateful for the financial support from the Royal Society, the European Research Council; ERC-2009-StG-240500-DEDIGROWTH; ERC-2011-PoC-309786-DEVICE; ERC-2015-PoC-680559-CONDUCT; ERC-2016-PoC-754748-OxfordNano (N.G.), the Engineering and Physical Sciences Research Council IAA block grants (N.G) and DTP EP/M508111/1 (K.E), and the U.S. Army Engineer Research and Development Center.

#### References

- [1] M.E. Launey, R.O. Ritchie, On the fracture toughness of advanced materials, *Adv. Mater.* 21 (2009) 2103–2110.
- [2] A.G. Evans, Perspective on the development of high-toughness ceramics, *J. Am. Ceram. Soc.* 73 (1990) 187–206.
- [3] R.O. Ritchie, The conflicts between strength and toughness, *Nat. Mater.* 10 (2011) 817–822.
- [4] J. Sun, B. Bhushan, Hierarchical structure and mechanical properties of nacre: a review, *RSC Adv.* 2 (2012) 7617–7632.
- [5] I. Corni, et al., A review of experimental techniques to produce a nacre-like structure, *Bioinspiration Biomimetics* 7 (2012).
- [6] M. André Meyers, P.-Y. Chen, *Biological Materials Science: Biological Materials, Bioinspired Materials, and Biomaterials*, Cambridge University Press, 2014.
- [7] J. Sun, B. Bhushan, Hierarchical structure and mechanical properties of nacre: a review, *RSC Adv.* 2 (2012) 7617–7632.
- [8] K. Okumura, P.-G. Gennes, Why is nacre strong? Elastic theory and fracture mechanics for biocomposites with stratified structures, *Eur. Phys. J. E* 4 (2001) 121–127.
- [9] K.S. Katti, D.R. Katti, Why is nacre so tough and strong? *Mater. Sci. Eng. C* 26 (2006) 1317–1324.
- [10] H. Gao, B. Ji, I.L. Jager, E. Arzt, P. Fratzl, Materials become insensitive to flaws at nanoscale: lessons from nature, *Proc. Natl. Acad. Sci. Unit. States Am.* 100 (2003) 5597–5600.
- [11] A. Dutta, S.A. Tekalur, Crack tortuosity in the nacreous layer - topological dependence and biomimetic design guideline, *Int. J. Solid Struct.* 51 (2014) 325–335.
- [12] H. Yao, Z. Song, Z. Xu, H. Gao, Cracks fail to intensify stress in nacreous composites, *Compos. Sci. Technol.* 81 (2013) 24–29.
- [13] Z. Huang, X. Li, Origin of flaw-tolerance in nacre, *Sci. Rep.* 3 (2013) 1693.
- [14] K.S. Katti, B. Mohanty, D.R. Katti, Nanomechanical properties of nacre, *J. Mater. Res.* 21 (2006) 1237–1242.
- [15] G. Dwivedi, K. Flynn, M. Resnick, S. Sampath, A. Gouldstone, Bioinspired hybrid materials from spray-formed ceramic templates, *Adv. Mater.* 27 (2015) 3073–3078.
- [16] X. Wang, et al., Synthesis of CaCO<sub>3</sub>/graphene composite crystals for ultra-strong structural materials, *RSC Adv.* 2 (2012) 2154.
- [17] T.P. Niebel, D. Carnelli, M.R. Binelli, R. Libanori, A.R. Studart, Hierarchically roughened microplatelets enhance the strength and ductility of nacre-inspired composites, *J. Mech. Behav. Biomed. Mater.* 60 (2016) 367–377.
- [18] F. Bouville, et al., Strong, tough and stiff bioinspired ceramics from brittle constituents, *Nat. Mater.* 13 (2014) 508–514.
- [19] H. Kakisawa, T. Sumitomo, The toughening mechanism of nacre and structural materials inspired by nacre, *Sci. Technol. Adv. Mater.* 12 (2011).
- [20] Z. Xia, L. Riester, W.A. Curtin, H. Li, B.W. Sheldon, Direct observation of toughening mechanisms in carbon nanotube ceramic matrix composites, *Acta Mater.* 52 (2004) 931–944.
- [21] S. Vasudevan, A. Kothari, B.W. Sheldon, Direct observation of toughening and R-curve behavior in carbon nanotube reinforced silicon nitride, *Scripta Mater.* 124 (2016) 112–116.
- [22] A. Zapata-Solvas, D. Gómez-García, A. Domínguez-Rodríguez, Towards physical properties tailoring of carbon nanotubes-reinforced ceramic matrix composites, *J. Eur. Ceram. Soc.* 32 (2012) 3001–3020.
- [23] L. Kumari, et al., Thermal properties of CNT-Alumina nanocomposites, *Compos. Sci. Technol.* 68 (2008) 2178–2183.
- [24] K. Ahmad, W. Pan, Dramatic effect of multiwalled carbon nanotubes on the electrical properties of alumina based ceramic nanocomposites, *Compos. Sci. Technol.* 69 (2009) 1016–1021.
- [25] K. Lee, C. Bin Mo, S. Bin Park, S.H. Hong, Mechanical and electrical properties of multiwalled CNT-alumina nanocomposites prepared by a sequential two-step processing of ultrasonic spray pyrolysis and spark plasma sintering, *J. Am. Ceram. Soc.* 94 (2011) 3774–3779.
- [26] G. Yamamoto, M. Omori, T. Hashida, H. Kimura, A novel structure for carbon nanotube reinforced alumina composites with improved mechanical properties, *Nanotechnology* 19 (2008) 315708.
- [27] N. Grobert, et al., Enhanced magnetic coercivities in Fe nanowires, *Appl. Phys. Lett.* 75 (1999) 3363–3365.

- [28] F.C. Dillon, et al., Tuning the magnetic properties of iron-filled carbon nanotubes, *Carbon N. Y.* 50 (2012) 3674–3681.
- [29] J. Cho, A.R. Boccaccini, M.S.P. Shaffer, Ceramic matrix composites containing carbon nanotubes, *J. Mater. Sci.* 44 (2009) 1934–1951.
- [30] I. Ahmad, B. Yazdani, Y. Zhu, Recent advances on carbon nanotubes and graphene reinforced ceramics nanocomposites, *Nanomaterials* 5 (2015) 90–114.
- [31] S. Sarkar, P.K. Das, Temperature and load dependent mechanical properties of pressureless sintered carbon nanotube/alumina nanocomposites, *Mater. Sci. Eng., A* 531 (2012) 61–69.
- [32] S. Rul, F. Lefevre-Schlick, E. Capria, C. Laurent, A. Peigney, Percolation of single-walled carbon nanotubes in ceramic matrix nanocomposites, *Acta Mater.* 52 (2004) 1061–1067.
- [33] S. Behr, U. Vainio, M. Müller, A. Schreyer, G. a. Schneider, Large-scale parallel alignment of platelet-shaped particles through gravitational sedimentation, *Sci. Rep.* 5 (2015) 9984.
- [34] P.M. Hunger, A.E. Donius, U.G.K. Wegst, Platelets self-assemble into porous nacre during freeze casting, *J. Mech. Behav. Biomed. Mater.* 19 (2013) 87–93.
- [35] D. Ghosh, M. Banda, H. Kang, N. Dhavale, Platelets-induced stiffening and strengthening of ice-templated highly porous alumina scaffolds, *Scripta Mater.* 125 (2016) 29–33.
- [36] M.T. Abba, P.M. Hunger, S.R. Kalidindi, U.G.K. Wegst, Nacre-like hybrid films: structure, properties, and the effect of relative humidity, *J. Mech. Behav. Biomed. Mater.* 55 (2016) 140–150.
- [37] H. Ohno, et al., Growth of vertically aligned single-walled carbon nanotubes on alumina and sapphire substrates, *Jpn. J. Appl. Phys.* 47 (2008) 1956–1960.
- [38] M.H. Rummeli, et al., Investigating the outskirts of Fe and Co catalyst particles in alumina-supported catalytic CVD carbon nanotube growth, *ACS Nano* 4 (2010) 1146–1152.
- [39] T.D.L. Arcos, et al., The influence of catalyst chemical state and morphology on carbon nanotube growth, *J. Phys. Chem. B* (2004) 7728–7734.
- [40] S. Noda, et al., Millimeter-thick single-walled carbon nanotube forests: hidden role of catalyst support, *Japanese J. Appl. Physics, Part 2 Lett.* 46 (2007).
- [41] K. Hasegawa, et al., Growth window and possible mechanism of millimeter-thick single-walled carbon nanotube forests, *J. Nanosci. Nanotechnol.* 8 (2008) 6123–6128.
- [42] J. Kong, A.M. Cassell, Chemical vapor deposition of methane for single-walled carbon nanotubes, *Chem. Phys. Lett.* (1998) 567–574.
- [43] C.S. Chen, C.K. Hsieh, Effects of acetylene flow rate and processing temperature on graphene films grown by thermal chemical vapor deposition, *Thin Solid Films* 584 (2015) 265–269.
- [44] D. He, J. Bai, Acetylene-enhanced growth of carbon nanotubes on ceramic microparticles for multi-scale hybrid structures, *Chem. Vap. Depos.* 17 (2011) 98–106.
- [45] M.H. Khedr, K.S.A. Halim, N.K. Soliman, Effect of temperature on the kinetics of acetylene decomposition over reduced iron oxide catalyst for the production of carbon nanotubes, *Appl. Surf. Sci.* 255 (2008) 2375–2381.
- [46] R. Soltani, M. Ali, F. Sani, F. Mohaghegh, The effect of temperature and N<sub>2</sub>: C<sub>2</sub>H<sub>2</sub> flow rate on the growth of carbon nanotubes synthesized by CCVD of acetylene on alumina – zirconia matrix, *Fullerenes, Nanotub. Carbon Nanostruct.* 23 (3) (2015) 245–252.
- [47] C. Ghemes, Synthesis of long and spinnable multi-walled carbon nanotubes, *J. Adv. Res. Phys.* 3 (2012) 2011–2013.
- [48] L. Bokobza, J.-L. Bruneel, M. Couzi, Raman spectra of carbon-based materials (from graphite to carbon black) and of some silicone composites, *C—Journal Carbon Res.* 1 (2015) 77–94.
- [49] F. Dillon, M. Copley, A. Ko, Flame Spray Pyrolysis Generated Transition Metal Oxide Nanoparticles as Catalysts for the Growth of Carbon Nanotubes, 2013, pp. 20040–20045, <https://doi.org/10.1039/c3ra40773j>.
- [50] E.F. Antunes, et al., Comparative study of first- and second-order Raman spectra of MWCNT at visible and infrared laser excitation, *Carbon N. Y.* 44 (2006) 2202–2211.
- [51] R.T.K. Baker, R.J. Waite, Formation of carbonaceous deposits from the platinum-iron catalyzed decomposition of acetylene, *J. Catal.* 37 (1975) 101–105.
- [52] M. Endo, Ishioka Munehire, Formation of vapor-grown carbon fibers in co-2-h<sub>2</sub> mixtures, I. Influence of carrier gas composition, *Carbon N. Y.* 30 (1992) 859–863.
- [53] M. Kumar, Y. Ando, Chemical Vapor Deposition of Carbon Nanotubes : A Review on Growth Mechanism and Mass Production, vol. 10, 2010, pp. 3739–3758.
- [54] C. Schu, B. Rellinghaus, K. Lafdi, L. Schultz, B. Bu, Catalyst Poisoning by Amorphous Carbon during Carbon Nanotube Growth : Fact or Fiction ?, 2011, pp. 8928–8934.
- [55] M.J. Behr, E.A. Gaulding, K.A. Mkhoyan, E.S. Aydil, Effect of hydrogen on catalyst nanoparticles in carbon nanotube growth, *J. Appl. Phys.* 108 (2010).
- [56] H. Ago, et al., Gas analysis of the CVD process for high yield growth of carbon nanotubes over metal-supported catalysts, *Carbon N. Y.* 44 (2006) 2912–2918.
- [57] R.T.K. Baker, D.J.C. Yates, J.A. Dumesic, Filamentous carbon formation over iron surfaces. *Coke form, Met. Surfaces* 202 (1982) 1–21.
- [58] G. Bertoni, et al., Growth of multi-wall and single-wall carbon nanotubes with in situ high vacuum catalyst deposition, *Carbon N. Y.* 42 (2004) 423–460.
- [59] C.T. Wirth, et al., The phase of iron catalyst nanoparticles during carbon nanotube growth, *Chem. Mater.* 24 (2012) 4633–4640.
- [60] Y. Homma, et al., Role of transition metal catalysts in single-walled carbon nanotube growth in chemical vapor deposition, *J. Phys. Chem. B* 107 (2003) 12161–12164.
- [61] J. Robertson, et al., Controlling the catalyst during carbon nanotube growth, *J. Nanosci. Nanotechnol.* 8 (2008).
- [62] B.T. Quinton, et al., Influence of oxide buffer layers on the growth of carbon nanotube arrays on carbon substrates, *Carbon N. Y.* 87 (2015) 175–185.
- [63] S. Hofmann, et al., In situ observations of catalyst dynamics during surface-bound carbon nanotube nucleation, *Nano Lett.* 7 (2007) 602–608.
- [64] P.B. Amama, et al., Role of water in super growth of single-walled carbon nanotube carpets, *Nano Lett.* 9 (2009) 44–49.
- [65] E.R. Meshot, Dynamics and Limiting Mechanisms of Self-Aligned Carbon Nanotube Growth, 2012.
- [66] Y. Homma, T. Yamashita, P. Finnie, M. Tomita, T. Ogino, Single-Walled carbon nanotube growth on silicon substrates using nanoparticle catalysts, *Jpn. J. Appl. Phys.* 41 (2002) L89–L91.
- [67] A. Kaneko, K. Yamada, R. Kumahara, H. Kato, Y. Homma, Comparative study of catalytic activity of iron and cobalt for growing carbon nanotubes on alumina and silicon oxide, *J. Phys. Chem. C* 116 (2012) 26060–26065.
- [68] M. Kumar, Y. Ando, Chemical vapor deposition of carbon Nanotubes : a review on growth mechanism and mass production, *J. Nanosci. Nanotechnol.* 10 (2010) 3739–3758.
- [69] P. Arnoldy, J.A. Moulijn, Temperature-programmed reduction of Co<sub>0</sub>/Al<sub>2</sub>O<sub>3</sub> catalysts, *J. Catal.* 93 (1985) 38–54.
- [70] J.A. Moulijn, A.E. Van Diepen, F. Kapteijn, Catalyst deactivation: is it predictable? What to do? *Appl. Catal. Gen.* 212 (2001) 3–16.
- [71] M.I. López, M.A. Meyers, The organic interlamellar layer in abalone nacre: formation and mechanical response, *Mater. Sci. Eng. C* 58 (2016) 7–13.